Geochemical insight during archaeological geophysical exploration through in situ X-ray fluorescence spectrometry

Adam D. Booth1 | Veerle Vandeginste2 | Dominic Pike3 | Russell Abbey3 | Roger A. Clark1 | Chris M. Green1 | Nathan Howland3

1 School of Earth and Environment, University of Leeds, Woodhouse Lane, Leeds LS2 9JT, UK
2 School of Chemistry, University of Nottingham, University Park, Nottingham NG7 2RD, UK
3Nuthampstead Airfield Museum, Bee Farm, Nuthampstead, Royston, Hertfordshire SG8 8NB, UK
Correspondence
Adam D. Booth, School of Earth and Environment, University of Leeds, Woodhouse Lane, Leeds, LS2 9JT, UK
Email: a.d.booth@leeds.ac.uk

Abstract
Geophysical techniques are widely applied in archaeological exploration, providing rapid and noninvasive site appraisal. Geochemical analyses contribute significantly in archaeometry, but conventional laboratory apparatus requires that samples are removed from their in situ context. Recent advances in field-portable apparatus facilitate in situ geochemical analysis, and this apparatus is deployed in this paper alongside conventional geophysical analysis to characterize the archaeological prospectivity of a site. The target is subsurface debris at the crash site of a World War II Mosquito aircraft.
A 100 m long transect of magnetic, electromagnetic (EM) and in situ X-ray fluorescence (XRF) measurements was acquired in November 2014, with soil samples also collected for laboratory validation. A subset of XRF measurements was repeated in August 2015 alongside a targeted grid, 900 m2 in area, of magnetic gradiometry profiles. Built chiefly from wood, the Mosquito responds weakly in magnetic and EM data; magnetic gradient anomalies of ±10 nT/m are instead attributed to thermoremanence in a burnt layer at 0.2–0.4 m depth, produced by the impact fire following the crash. XRF spectrometry reveals co-located enrichments in copper (Cu) and zinc (Zn) ions (400% and 200%, respectively, above background). These metals are alloyed into brass, present in abundance in the ammunition on board the Mosquito. Records from the in situ XRF sampling compare well with laboratory validated data, although a bespoke calibration for the local soil type would improve the reliability of absolute geochemical concentrations. XRF responses vary significantly with ground conditions: the November 2014 acquisition was performed soon after ploughing at the site, potentially providing a fresh charge of metallic contaminants to the ground surface. Where the chemistry of a target is anomalous with respect to host soil and a source-to-surface transport mechanism is present, in situ XRF analysis offers improved understanding of a target compared to geophysical interpretation alone.

KEYWORDS
air crash, conflict archaeology, geochemistry, geophysics, magnetometry, XRF spectrometry

1 | INTRODUCTION

The detection and delineation of archaeological targets is often based on contrasts in the subsurface distribution of physical properties (density, electrical conductivity, magnetic susceptibility, etc.). The chemical composition of the target is typically of secondary importance, and it usually suffices to observe a response consistent with

(for example) a metallic target rather than identifying the specific metallic elements involved. However, an understanding of geochemistry could add significant archaeological value, particularly where a given practice is linked to a specific chemical element (e.g. industrial processes that leave a diagnostic abundance of marker elements; Millard, 1999; Jones, 2001; McKenzie & Pulford, 2002; White & Dungworth, 2007). While geochemical analyses are routine in archaeometry, applied to study the composition of (for example) glass (Aidona, Sarris, Kondopopulou, & Sanakis, 2001; Falcone, Renier, & Vertià, 2008), paint (Bonizzoni, Bruni, Guglielmi, Milazzo, & Neri, 2011) and ceramic (Aidona, Sarris, Kondopopulou, & Sanakis, 2001; Cultrone, Molina, Grifa, & Sebastián, 2011), their use in archaeological exploration has not been widely reported.

Among the advantages of most geophysical methods is the in situ and non-destructive nature of survey. By contrast, geochemical analyses are usually conducted in the laboratory, on prepared (often destroyed) samples of material extracted from a site (e.g. Dungworth, 1997; Wilson, Davidson, & Cresser, 2008; Cook et al., 2010; Dirix, Muchez, Degryse, Mušič, & Poblome, 2013; Vittori Antasari, Cremonini, Desantis, Calastri, & Vianello, 2013; Carey, Wickstead, Juleff, Anderson, & Barber, 2014; Scott, Eekelers, & Degryse, 2016). In situ geochemical analysis using X-ray fluorescence (XRF) spectrometry has become possible, however, with the development of handheld, field-portable XRF analysers (e.g. Lu, Wang, Pan, Han, & Han, 2010; Schneider et al., 2016). Such in-field equipment is particularly valuable in forensic cases (e.g. Bergslien, 2013) since the material under investigation must be uncontaminated by any sampling process. The use of field-portable XRF spectrometers is reported for archaeological applications (e.g. Del Solar Valarde, Kinis, Chapoulie, Joannes-Boyau, & Castillo, 2016; Fernandes, van Os, & Huisman, 2013; Sepúlveda et al., 2015; Shugar, 2013) but seldom using a sampling strategy consistent with standard geophysical survey (i.e. spot samples are considered, rather than systematically-defined areas and/or transects).

Here, in situ XRF spectrometry is applied as part of a conventional deployment of magnetic and electromagnetic (EM) methods to characterize a potential archaeological site, specifically the crashsite of a World War II aircraft. The additional geochemical insight reduces the ambiguity in the interpretation of the geophysical data: geophysical anomalies are co-located with enriched concentrations of copper and zinc ions, associated with brass (copper–zinc) alloy in the aircraft's ammunition. The in situ data compare favourably to XRF and mass spectrometry applied under laboratory conditions, but the same survey locations show variability given the changing supply of chemical elements to the ground surface. In situ XRF spectrometry can offer a valuable complement to a campaign of exploratory field geophysics, but only under certain site conditions as considered in the discussion.

2 | X-RAY FLUORESCENCE (XRF) SPECTROSCOPY – FUNDAMENTAL THEORY

XRF spectroscopy determines the elemental composition of a sample material using high-energy, short-wavelength (X-ray) radiation (note: spectroscopy and spectrometry are distinct; the former is a technique, whereas the latter is the quantitative analysis of data). When

bombarded with X-ray radiation, different elements can be identified by the characteristic ‘fluorescent’ energy that they emit (Weltje & Tjallingil, 2008).

XRF responses are adversely affected by several factors, including matrix composition (Hall, Bonham-Carter, & Buchar, 2014; Quye-Sawyer, Vandeginste, & Johnston, 2015), surface morphology (Forster, Grave, Vickery, & Kealhofer, 2011; Potts, Webb, & Williams, 1997; Shugar, 2013) and instrumental sensitivity (Weltje & Tjallingil, 2008). Matrix composition effects are mitigated using manufacturers' calibrations for representative materials (e.g. mudrock, glass, alloys, etc.). Although challenging to define, bespoke calibrations can be made (Quye-Sawyer et al., 2015; Scott et al., 2016) and allow the XRF data to be used as an absolute rather than relative indicator of composition (Środoń, Drits, McCarty, Hsieh, & Eberi, 2001). Laboratory XRF practice mitigates the effects of surface morphology by (destructively) grinding samples into a fine powder. Equivalent sample preparation is impractical for in situ XRF spectrometry hence field-portable XRF instruments have faced scepticism in the geochemical community (Frahm, 2013). However, recent research (e.g. Schneider et al., 2016) has reported similar accuracy and precision between field- and laboratory-based observations.

The instrument deployed here is a hand-held Bruker Tracer IV-SD spectrometer (Figure 1), an energy-dispersive instrument with a rhodium target. The detection of elements lighter than calcium can be challenging since these have a low ‘fluorescence yield’ (i.e. their energy emissions are weak; Krause, 1979; Berlin, 2011), but this is overcome here with the use of a silicon drift detector (Speakman, Little, Creel, Miller, & Inanez, 2011). Sensitivity is further improved by including a Bruker 3 V Vacuum Pump (Figure 1) to inhibit the attenuation of fluorescent energy by air in the spectrometer's analysis chamber. The presence of water also impedes XRF analysis, since water scatters the X-ray radiation; therefore, in situ XRF surveys may always be vulnerable to the presence of groundwater (e.g. Tjallingil, Röhl, Kölling, & Bickert, 2007), especially for low-yield elements.

The sample area (spot size) of an XRF measurement is typically 1 cm in diameter. However, the depth penetration of XRF energy in soil is on the millimetre-to-centimetre scale, hence in situ XRF measures only the surface chemistry of host soil. While it may be detectable with geophysical methods, a target would therefore be invisible to XRF sampling unless the ground surface is enriched in relevant marker elements via some source-to-surface transport mechanism (e.g. ploughing, groundwater circulation; Hedges & Millard, 1995; Campana, 2009). Even then, such transport may not only be in a vertical direction hence the strongest concentrations of ions may not be observed directly above the source. As such, in situ XRF prospection will probably always benefit from the constraint provided by conventional geophysical survey.

FIGURE 1 A Bruker Tracer IV-SD hand-held XRF spectrometer, deployed at Nuthampstead airfield (August 2015). Here, the Bruker spectrometer is held in the operator's right hand, and the 3 V Vacuum Pump in their left [Colour figure can be viewed at wileyonlinelibrary.com]

3 | FIELD SURVEY

This study is located within Nuthampstead Airfield (Hertfordshire, UK; National Grid Reference TL419347), over the suspected crash site of a World War II aircraft (Figure 2). A local borehole, BGS TL43NW39 (Figure 2a, UK National Grid Reference TL 41404 35166), shows surface soils are clay-rich, beneath which is stiff clay to a depth of at least 40 m with occasional flint and chalk cobbles (BGS, 2014). The underlying solid geology – the Lewes and Seaford Chalk formations – is observed at ~70 m depth. Surveys over the likely crash site were undertaken in November 2014 and August 2015, in support of investigations conducted at the site by Nuthampstead Airfield Museum.

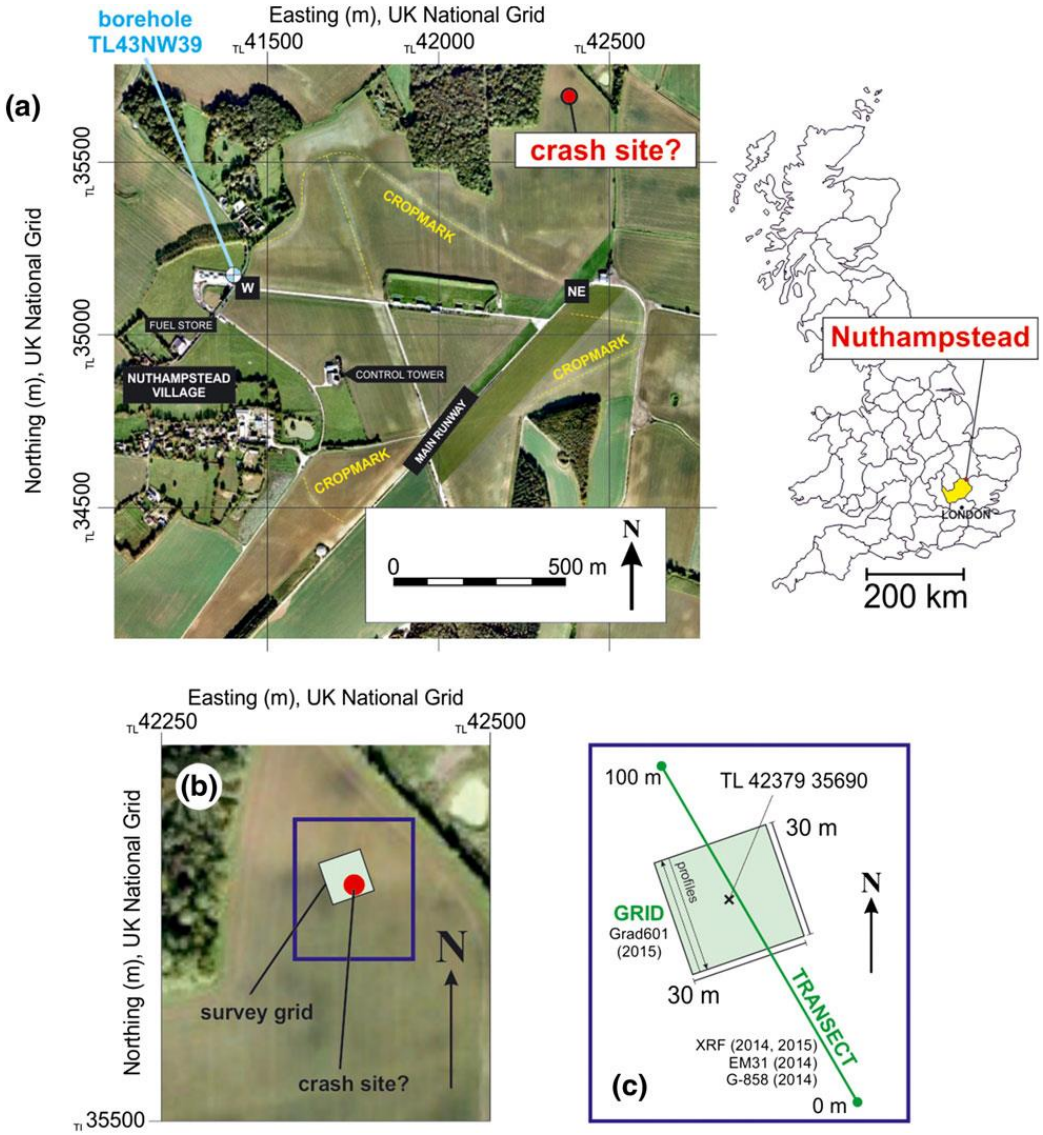

FIGURE 2 Survey site. (a) image of Nuthampstead airfield, © Google Earth. Runways and buildings from the original airfield remain present today, with other infrastructure visible as cropmarks. The approximate location of the crash site is marked with a red spot, with the location of BGS boreholeTL43NW39 also indicated. (b) zoomed window of the crash site. (c) location of geophysical and XRF surveys conducted at Nuthampstead airfield, during 2014 and 2015 [Colour figure can be viewed at wileyonlinelibrary.com]

The specific aircraft believed to have crashed at the site is a de Havilland DH.98 Mosquito Mark VI 'LR343'. In February 1944, at the time of the crash, Nuthampstead Airfield was operated by the US Army Air Force; it returned to British control in 1945, and was decommissioned and returned to agricultural use in 1959. The Mosquito crashed in the grounds of Nuthampstead shortly after its take-off from RAF Hunsdon (also in Hertfordshire). Records suggest that the port engine detached from the aircraft, causing it to invert and impact the ground at a near-vertical angle. The crash caused an intense fire, and claimed the lives of the two crewmen (members of 487 Squadron Royal New Zealand Air Force). Their bodies were recovered from the site, along with some wreckage, but it is doubtful that all debris was cleared from the site and some components

(including armaments and the starboard engine) may remain present today.

The airfield has been extensively ploughed, but runways still remain and evidence of military infrastructure are present as cropmarks. The likely crash site has been identified by Nuthampstead Airfield Museum using contemporary photographs of the impact (e.g. Figure 3a) plus a local concentration of surface finds identifiable as Mosquito wreckage (Figure 3b). An exploratory geophysical survey was therefore conducted, in November 2014, to investigate this hypothesis (Figure 2c): magnetic gradiometer and EM methods were deployed along a transect over the hypothesized crash site. The opportunity also arose to deploy in situ XRF analysis alongside the geophysical methods. Promising initial results from the XRF survey motivated a second acquisition in August 2015, in which a repeat set of XRF measurements and a larger grid of magnetic data was acquired (Figure 2c).

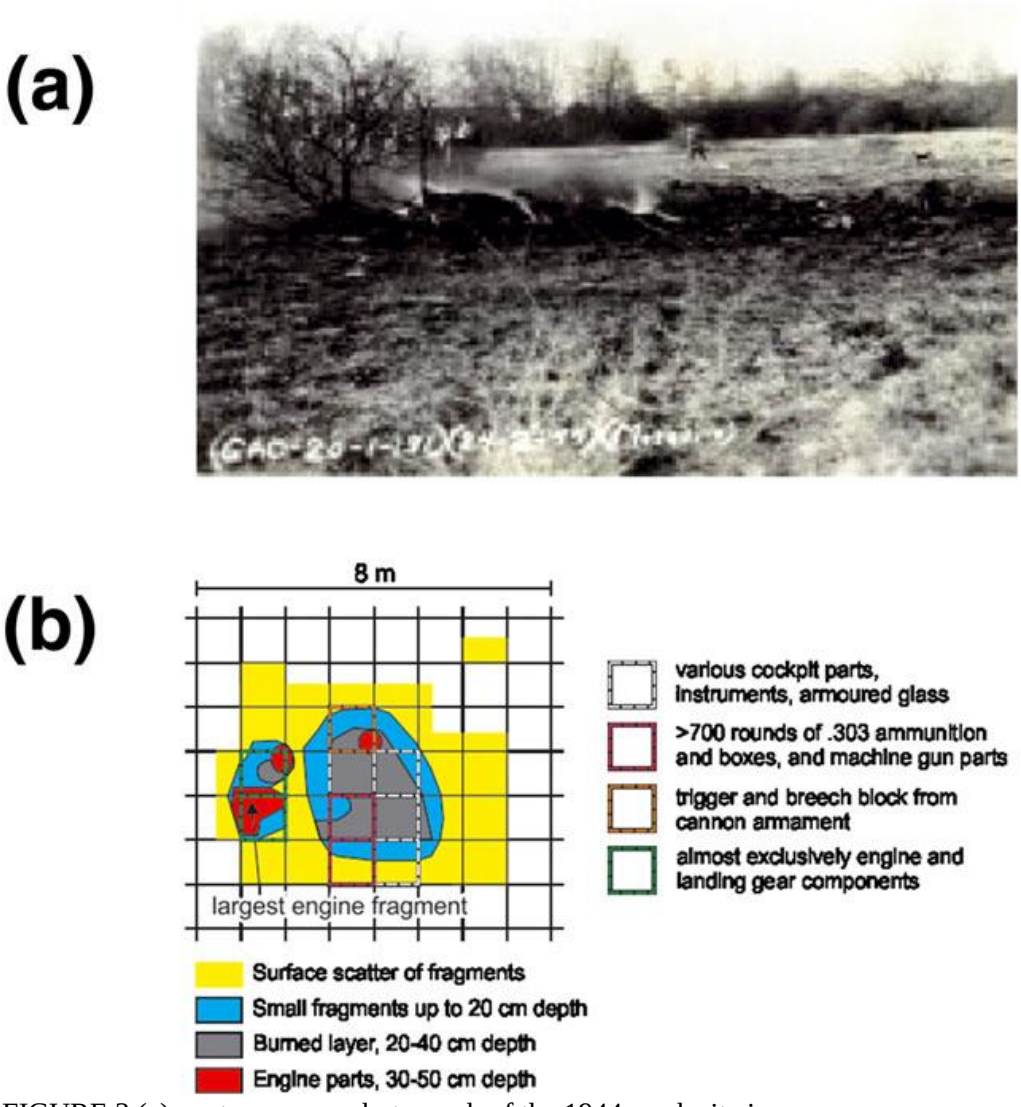

FIGURE 3 (a) contemporary photograph of the 1944 crash site in Nuthampstead airfield. (b) distribution of fragments identifiable as wreckage of a de Havilland Mosquito aircraft, both at surface and following shallow excavation. The map is centred on the crash site marked in Figure 2a [Colour figure can be viewed at wileyonlinelibrary.com]

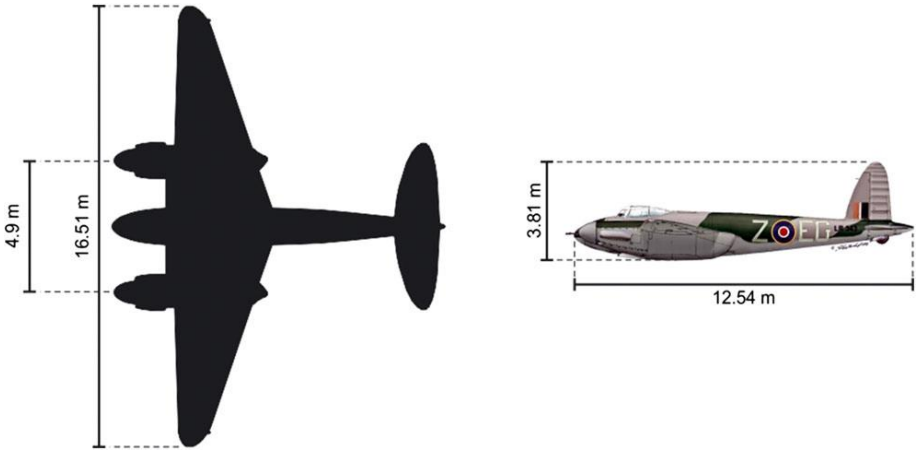

FIGURE 4 Dimensions of the de Havilland Mark IV Mosquito, in (left) plan and (right) side views [Colour figure can be viewed at wileyonlinelibrary.
com]

Before describing these surveys in more detail, the detectability of the Mosquito aircraft is considered; first by geophysical survey, then through geochemical analysis.

3.1 | Geophysical detection of the target

The wingspan of a Mark VI Mosquito is 16.5 m, and it is 12.5 m noseto-tail. In horizontal flight, the tip of its fin and rudder is 3.8 m above the base of its belly (Figure 4). The speed and steep angle of impact into soft clay soil suggests that any remaining components of the Mosquito could be buried several metres beneath the surface, although evidence for the potential depth is very sparsely reported.

Most surveys for aircraft wreckage can exploit the presence of aluminium and/or steel in the ground (i.e. relying on contrasts in electrical and/or magnetic properties; e.g. Osgood, 2014), but the Mosquito was one of the few World War II aircraft to be made chiefly of wood. Aluminium is only used in the rudder and elevator and, at this site, the steel engine and armaments may not be present. Therefore, in addition to any remaining aircraft components, it was assumed that magnetic surveying could respond to any thermoremanent magnetic signature of the impact fire. Despite ~55 years of ploughing at the site, trial excavations suggested that a layer of intense burning remains present at 0.2–0.4 m depth (Figure 3b). Melted aluminium fragments are among the debris observed at the site hence the temperature of the fire must have exceeded 660°C, the melting point of aluminium. This exceeds the temperature at which iron minerals in the soil transform into ferrimagnetic iron oxides (200–400°C; Schwertmann & Taylor, 1989; Hanesch, Stanjek, & Petersen, 2006), and then approaches the Curie temperature for haematite (675°C; Herz & Garrison, 1998). Magnetic survey methods were therefore prioritized, with additional EM surveys in case of remaining metallic debris.

3.2 | Geochemical detection of the target

With little precedent for similar XRF practice, it was initially unclear which elements could diagnose the crash site. While aluminium enrichment might ordinarily be consistent with buried aircraft wreckage, this is unlikely to be significant for the wooden Mosquito. Additionally, any small aluminium anomaly may be masked by the high background aluminium

content in Nuthampstead's clay soil and, furthermore, attenuated by groundwater. To identify alternative geochemical targets, the XRF characteristics of surface debris from the putative crash site were considered, including:

1. brass ammunition cartridges: British cartridge brass from the World War II period, used in 0.303 ammunition, is an alloy of 70% copper and 30% zinc, occasionally containing small quantities of lead (Pb). Cartridges may also have jacket of cupronickel alloy. None of the cartridges recovered show signs of melting (the melting point of most brass alloys exceeds 900°C), but all had exploded.
2. cannon rounds: this ammunition is made principally from steel, possibly alloyed with a nickel–chromium–molybdenum (Ni–Cr–Mo) blend. British aircraft carried several variants: armour-piercing ammunition may be tipped with a tungsten (W) carbide alloy, whereas explosive and incendiary variants haveTNT and phosphorous (P) cores, respectively.
3. burnt wood: although dominated by light elements (e.g. carbon, oxygen), traces of heavier elements, such as lead, could be present in any paint residue.

In addition to these fragments, a sample of burnt soil was tested to monitor any chemical alteration caused by the impact fire.

Figure 5 shows the concentrations of elements in the debris fragments, expressed in parts per million (on a log scale due to the variability between elements). All XRF analyses use a ‘trace mudrock’ calibration for which the spectrometer operates at 40 kV. This manufacturer-defined setting was the most appropriate for Nuthampstead's clay rich soil, though this implies that the measured concentrations are relative rather than absolute indicators. Elements lighter than calcium and those too scarce to be detected (e.g. molybdenum, tin, antimony), are absent from this plot. Each concentration is compared to a background value (orange bars, Figure 5), with error bars spanning the observed concentration range. This background value is defined for each element as the mean concentration recorded along the transect in a subset of locations outside the magnetic survey grid (Figure 2c, omitting transect positions at 45–75 m). While it is possible that background concentrations are influenced both by any unknown land use at the site and the crash itself, this subset of samples is at least outside of the area of surface-scattered fragments. As such, these concentrations define a local background to which observed geochemical anomalies can be compared.

The brass sample (green, Figure 5) is dominated by copper, with concentration exceeding 105 ppm. A high zinc fraction is also recorded (~80,000 ppm), with arsenic (As) and nickel also increased in abundance. The steel sample is iron-enriched, although with a surprisingly low concentration of ~250,000 ppm. The low value could again indicate a calibration issue, or non-ideal conditions of the sample surface caused by corrosion (Dungworth, 1997; Scott et al., 2016). Lead is somewhat enriched in both metallic samples, but in very low concentrations which may approach the limit of instrumental sensitivity. The burnt wood sample is generally depleted in metallic elements although no element is obviously enriched against the background trend. The burnt soil samples show little significant alteration with respect to background.

Despite the vulnerability to calibration effects, any geochemical

anomaly presented by the Mosquito would likely be in elements associated with brass, specifically copper and zinc. In addition to ammunition, the Mosquito was held together with ~50,000 brass screws, therefore brass may be highly abundant in the ground. While iron could also have been an attractive target, the concentrations of copper and zinc are more significant above the background geochemistry, and its associated variability, in our observations at Nuthampstead.

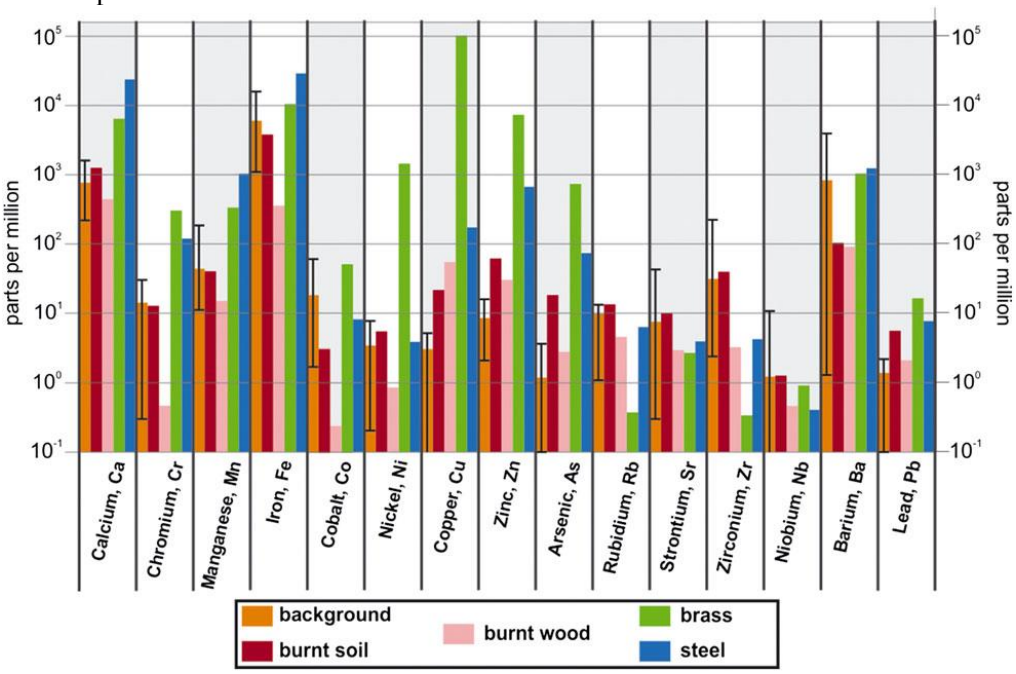

FIGURE 5 Measured concentration of elements in XRF analysis of samples of burnt soil (red), burnt wood (pink), brass (green) and steel (blue) from the Nuthampstead site, compared to background geochemistry (orange) [Colour figure can be viewed at wileyonlinelibrary.com]

3.3 | Survey procedure

Surveys in November 2014 were conducted along a transect, 100 m in length, which intersected the suspected crash site at a distance of 50 to 60 m (Figure 2c). Geophysical surveys were conducted with a Geonics G-858 caesium vapour magnetic gradiometer and a Geonics EM31 electrical conductivity meter. Both instruments were used in a 'continuous' recording mode, resulting in an along-transect sampling interval of ~0.1 m. The two sensors of the G-858 were mounted at 0.4 m and 1.2 m above the ground. The EM31 was carried at a height of 1.1 m, with the antenna boom orientated parallel to the transect; electrical conductivity and in-phase components of the EM31 response were recorded, since in-phase anomalies are particularly indicative of buried metal (McNeill, 1983). XRF measurements were conducted with the Bruker spectrometer along the transect at intervals ≤2.5 m, with each position irradiated for approximately one minute. Soil samples were also taken from each XRF survey position for laboratory validation. Laboratory XRF analysis was conducted with the Bruker spectrometer on soil samples that were kiln-dried for several days, at 60°C, then ground with a pestle and mortar. Selected samples (17 in total) were also analysed by inductively coupled plasma mass spectrometry (ICP-MS). ICP-MS is regarded as a more precise means of quantitatively measuring elemental composition than XRF

(Pye & Croft, 2007), being less vulnerable to calibration issues, but requires more extensive preparation of samples. Aliquots of 100 mg of dried-and-ground soil were dissolved in 5 ml of hot Aqua Regia (37% hydrochloric acid and 68% nitric acid, in a molar ratio of 3:1) at 140°C for one hour. A dilution series of 1:100 was made in 2% nitric acid and analysed for elemental concentrations on an Agilent ICP-MS instrument. Quartz minerals can be resistant to dissolution in Aqua Regia hence differences can exist between compositions evaluated through ICP-MS and XRF analysis of dissolved and undissolved samples. However, the samples in this experiment appeared to be completely dissolved in the Aqua Regia, therefore measurements with the two systems should be comparable. Additionally, for the elements considered in this study, comparisons were made of reported XRF versus Aqua Regia digestion ICP-MS measurements for standard soil samples: no significant differences between the two methods was observed for any element.

During August 2015, a grid of dimensions 30 m Å~ 30 m (Figure 2c, British National Grid coordinate [542379 mE, 235690 mN]) was acquired with a Bartington Grad601 vertical component fluxgate gradiometer. Grid profiles were separated by 1 m, orientated along bearing 341°/161° with an along-profile sampling interval of ~0.1 m. The transect was resurveyed with the XRF spectrometer between distances of 40 to 80 m (i.e. the span of the grid along the transect) at a sample resolution of 1 m.

Ground conditions during the two surveys were markedly different. In November 2014, the site had recently been ploughed and sown with a crop of winter barley. The survey followed a period of heavy rain and the soil was waterlogged. By contrast, the August 2015 survey took place after prolonged warm weather: the field was dry and dusty, and covered with the stubble of a barley crop (Figure 1).

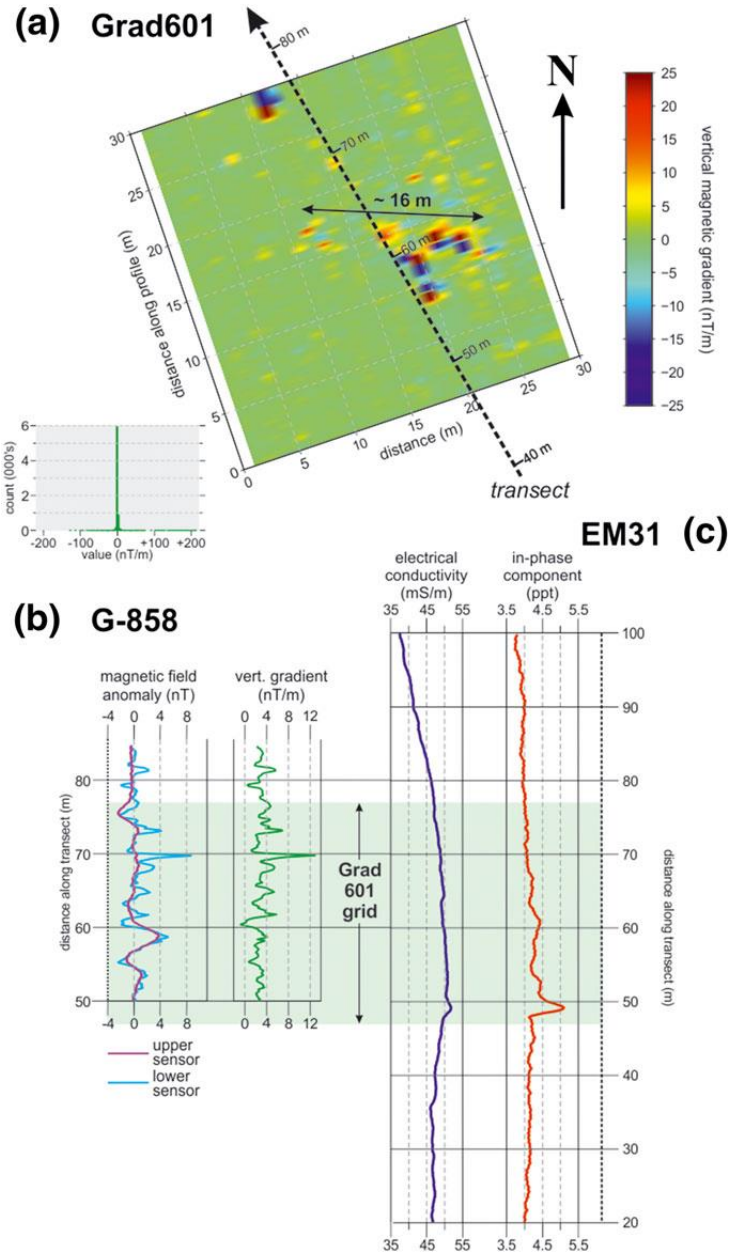

FIGURE 6 Geophysical observations from the Nuthampstead survey site. (a) grid of vertical magnetic gradient observations made with Grad601 instrument. Striping between survey lines (~4 nT/m variation) is suppressed by removing the mean value in each profile. Inset: Histogram of observations. (b) magnetic field observations made along the transect with G-858. (c) observations of electrical conductivity and in-phase component made with EM31. Grey shading in (b) and (c) shows position of Grad601 grid [Colour figure can be viewed at wileyonlinelibrary.com]

3.4 | Geophysical surveys

Figure 6 shows a compilation of geophysical observations from the two surveys. A magnetic anomaly is detected with the Bartington

Grad601, specifically in the eastern half of the survey grid close to the hypothesized crash site. The anomaly appears elongated in an east–west orientation, extending 16 m across the profiles of the grid. The typical magnetic gradient anomaly in this region has a magnitude of ±10 nT/m (against a mean background of approximately -1 nT/m) but exceeds ±100 nT/m in certain profiles (e.g. at 19 m).

Two prominent anomalies are also detected with the G-858 magnetometer. A total field anomaly of ~4 nT is observed in both of the instrument's sensors between 55 and 60 m along the transect, and in the lower sensor at 70 m. The response from the lower sensor contains more short-wavelength responses, likely arising from the increased proximity to the surface scatter of debris. However, both anomalies are consistent with responses in the Grad601 grid. The position of the broader anomaly conforms with the main anomaly in Figure 6a, and a local 'blip' in the Grad601 grid is also observed 70 m along the transect.

No anomalies are observed in either component of the EM31 record at a location consistent with the magnetic anomalies. The stability of conductivity and in-phase responses (~50 mS/m and 4 ppt, respectively) in the vicinity of the magnetic anomaly suggests that there are no large metallic fragments buried along the transect (at least within the few metres of EM31 depth sensitivity).

3.5 | In situ XRF spectrometry

Figure 7a shows the variation in XRF responses observed along the transect in the November 2014 survey (for selected elements; the full suite is available in Supporting Information). The lines in each plot are a three-point moving median trend; light and dark shading corresponds respectively to the span of the Grad601 grid and the extent of the magnetic anomaly (56–62 m along the transect). An enrichment anomaly is observed for copper ~60 m along the transect, with peak values 400% above the 50 ppm background concentration. A moderate zinc anomaly is perceived at ~60 m with a peak approaching 200 ppm (< 200% above the background of ~100 ppm). Weaker evidence of an anomaly in arsenic concentrations is also observed. While other elements show no consistent trend other than a steady distribution across the transect, iron appears to become more scattered in the most northerly 30 m of the transect, with greater variation (exceeding 100,000 ppm) about the background. For the repeat acquisition in August 2015 (Figure 7b), background concentrations show a comparable magnitude to the earlier archive, but copper, zinc and arsenic in particular show greater scatter about the median trend; yet copper appears to be consistently enriched ~60 m along the profile. However, changes in the observed concentrations suggest a fundamental control of ground conditions which is revisited in the discussion section.

If the geochemical anomalies share a common source, it may be expected that their concentrations are correlated at positions along the transect. Following Bergslien (2013), correlation was classified using Spearman's rank correlation coefficient (rs). Figure 8 shows the correlation between different elements, with symbols coloured according to their distance along the transect. The frames

in each plot are coloured according to the strength of correlation: green defines a strong correlation (rs > 0.65), red a moderate correlation (0.45 < rs < 0.65) and black a weak correlation (rs < 0.45) as no correlation. For clarity, only correlations between copper, zinc and lead are shown (others are included in Supporting Information Figure S1). For the 2014 archive (upper-right quadrant), strong correlations are observed between copper and zinc; the strongest correlations are observed 50–70 m along the transect (magenta and red symbols). Correlations are all reduced in the 2015 dataset (lower-left quadrant), attributable to the higher degree of scatter in the observed concentrations. Nonetheless, a moderate correlation is still perceived between the concentrations of copper and zinc, in the 50–70 m division of the plots.

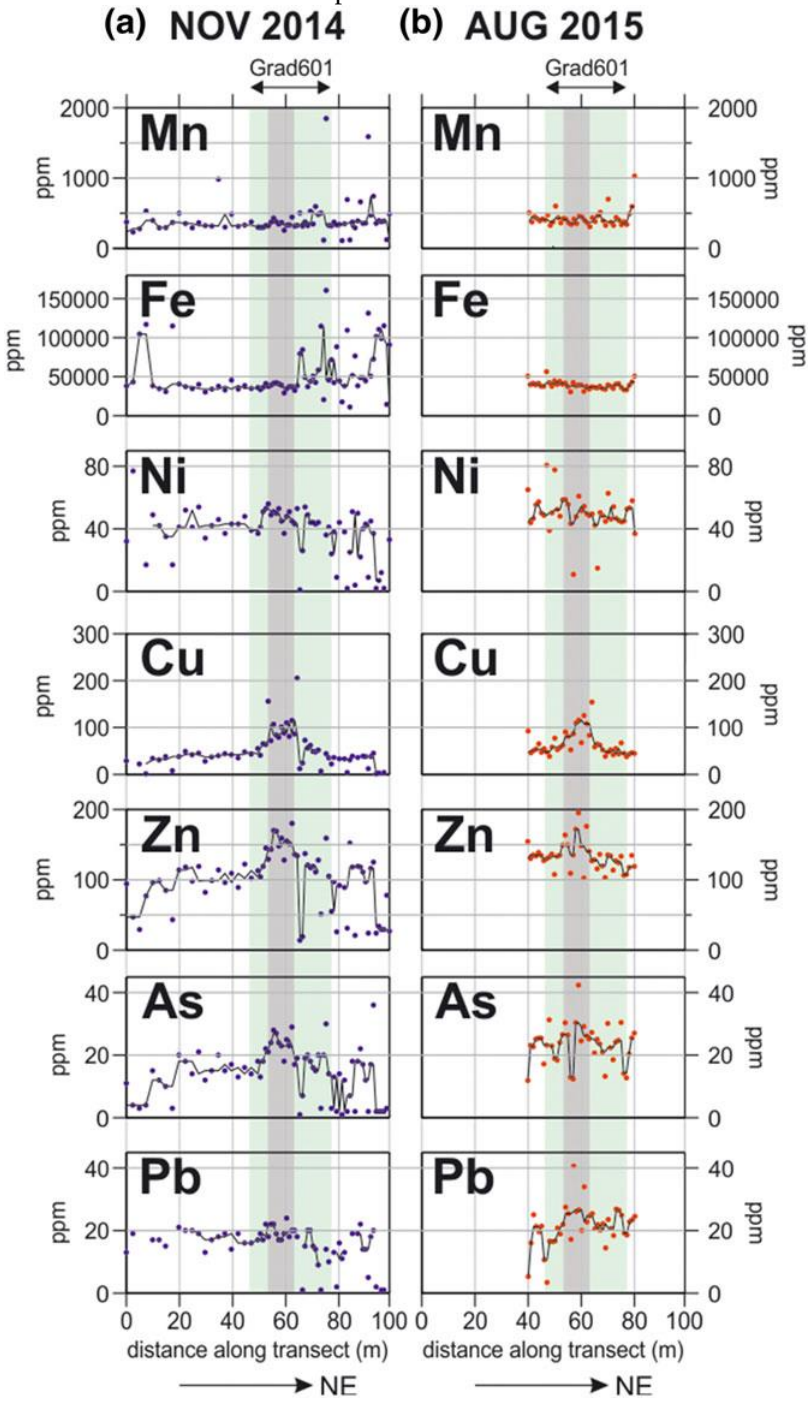

FIGURE 7 XRF responses along the Nuthampstead transect from (a) November 2014 and (b) August 2015. The black line through each plot is a three-point moving median trend. Shaded sections show (light) the intersection with the Grad601 grid (Figure 6a) and (dark) the span of the magnetic anomaly [Colour figure can be viewed at wileyonlinelibrary.com]

3.6 | Laboratory XRF and ICP-MS spectrometry

Figure 9 shows results from laboratory XRF and mass spectrometry analysis of soil samples, recovered along the transect during the November 2014 survey. ICP-MS analysis can be extended to aluminium, hence Figure 9b includes an aluminium response. Laboratory XRF data (Figure 9a) are broadly consistent with results from the in-field survey, with anomalies identifiable in copper, zinc and arsenic. Copper and zinc show anomalies approaching 150 ppm above background values (~50 ppm and ~130 ppm, respectively); the weaker arsenic anomaly reaches ~30 ppm above a background of 25 ppm. However, concentrations recorded for all elements show considerably less variation about their median trend than for either archive of in situ data. For example, the root-mean-square variability of in situ copper observations about their median trend is 25 ppm, but this reduces to 7 ppm for the laboratory analysis.

Concentrations determined through ICP-MS analysis (Figure 9b) are of the same order of magnitude as the equivalent XRF data, but differences in base-levels (evident for nickel, copper, zinc and arsenic) are evident. These are attributed to the inappropriate calibration of the XRF survey, implying that these in situ surveys should be considered relative rather than absolute indicators of concentration. Nonetheless, anomalies in copper and zinc remain well-defined, ~60 m along the transect, but trends in arsenic and lead are inconsistent. A lead anomaly is distinct in the ICP-MS record, approaching ~20 ppm above background. The XRF energies for arsenic and lead are very similar: 10.543 keV for Kα for arsenic and 10.551 keV for Lα for lead. Therefore, the spectral interference between these elements makes it challenging for XRF to distinguish between arsenic and lead, particularly at low concentrations. As such, the XRF anomaly in arsenic is likely a false positive. Lead is feasibly associated with the crash, since World War II aircraft were balanced using lead weights.

It is worth noting that ICP-MS gives evidence of an aluminium anomaly. While the variability of the observed concentrations impedes its definition, aluminium concentrations appear consistently high 60–70 m along the transect, approaching 10,000 ppm (~5%) above background.

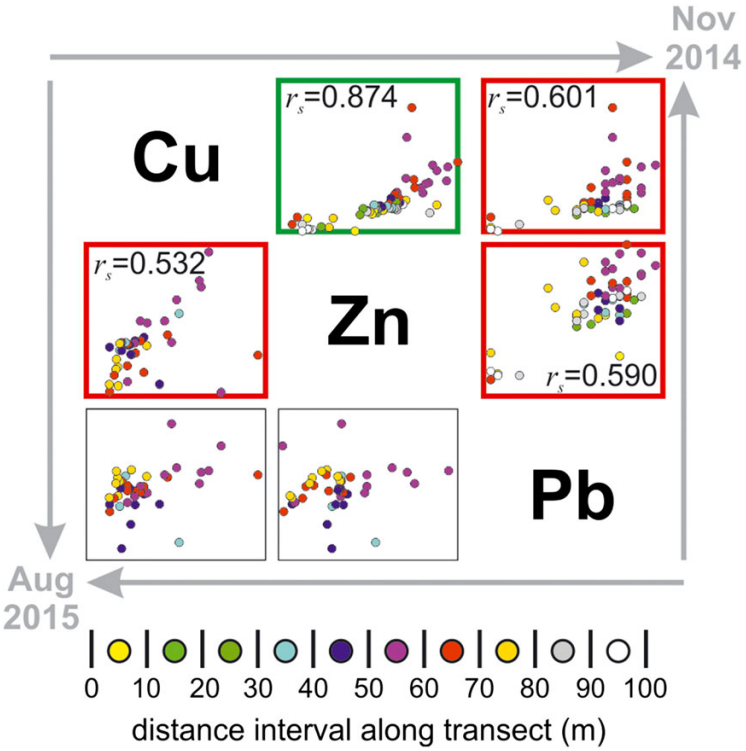

FIGURE 8 Scatterplots of paired elemental data from in situ XRF surveys in (upper-right quadrant) November 2014 and (lower-left quadrant) August 2015. Scatterplot frames are coloured according to Spearman's rank correlation coefficient, rs; green, red and black frames correspond respectively to rs > 0.65, 0.45 < rs ≤ 0.65, and rs ≤ 0.45 [Colour figure can be viewed at wileyonlinelibrary.com]

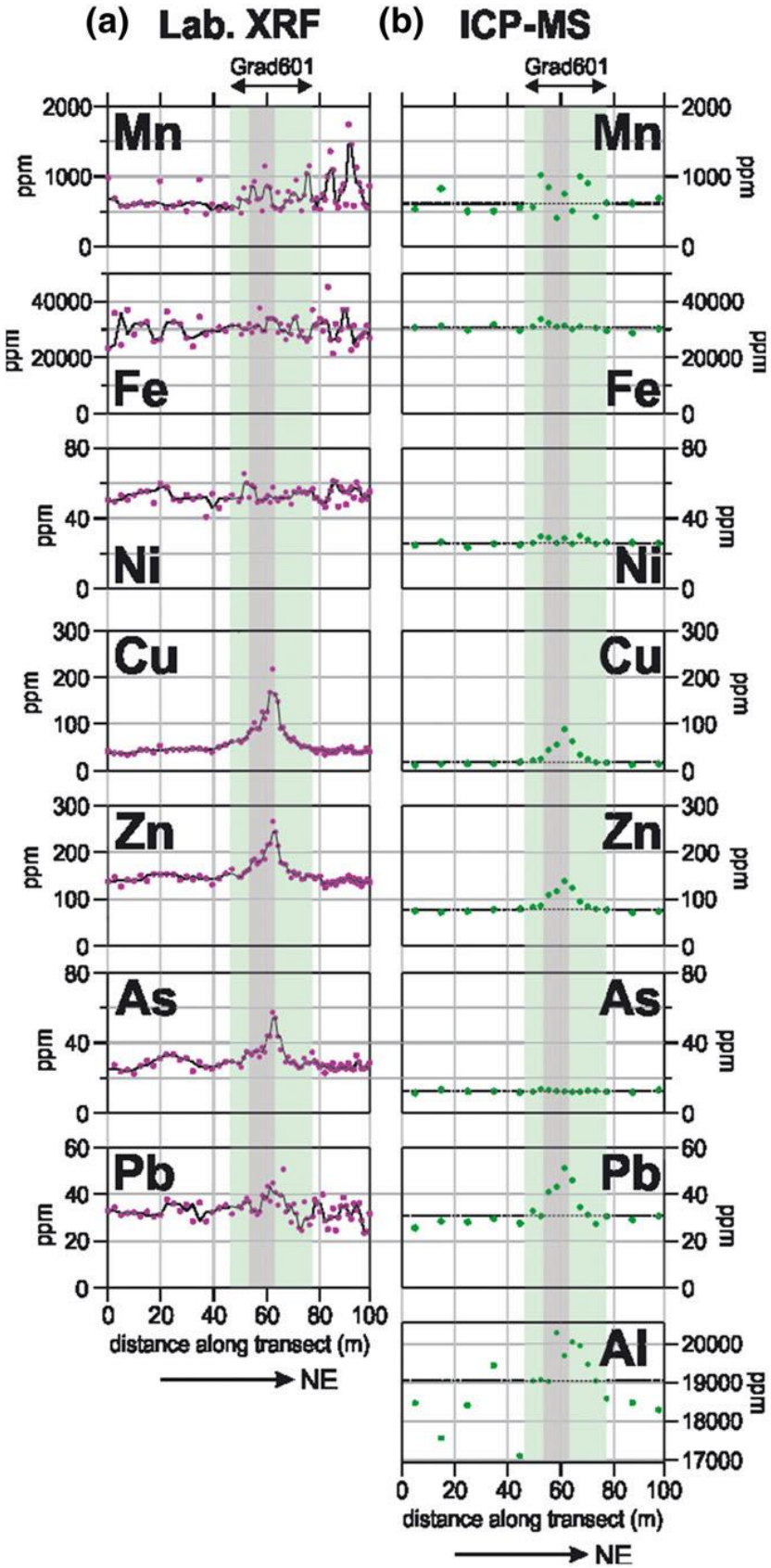

FIGURE 9 Laboratory validation of in-field XRF spectrometry data. (a) laboratory analysis of handheld XRF following grinding of dried soil samples, again including a three-point median trend. b) concentrations as measured in ICP-MS analysis (including for aluminium, absent in previous XRF analysis). The dashed black line in these plots is the

median average value for each element; error bars in ICP-MS analysis are smaller than the symbol [Colour figure can be viewed at wileyonlinelibrary.com]

4 | INTERPRETATION AND DISCUSSION

4.1 | Crash site prognosis

Significant geophysical and geochemical anomalies (Figures 6 and 7) are observed at the study site, which appear consistent with an aircraft crash at this location. Specifically, these are a widespread magnetic anomaly and enriched concentrations of elements associated with brass alloy.

The low-amplitude magnetic anomalies observed in both the Grad601 grid and the G-858 transect are interpreted as the response to the thermoremanence in burnt clay. Assuming a near-vertical impact, the area of this response is not inconsistent with the footprint of the Mosquito (~16 m Å~ 4 m), which would have been affected by the impact fire. Additionally, the power spectrum of the G-858 response indicates that the magnetic source is located within 1 m of the ground surface, based on modelling the burnt layer as a thin layer with random magnetization. Spector and Grant (1970) show that for a verticallyextended random magnetic layer, the slope of linear sections of a power spectrum of log-power versus wavenumber (= 1/wavelength) is a factor of 4π times the source depth. Figure 10 shows the spectrum for the upper sensor of the G-858 (Figure 6b), mounted at ~1.2 m from the ground; this power spectrum has been modified for thin layer sources. The spectrum contains three linear sections, the first of these (i, wavenumber <0.6 m-1) has a gradient of -24.7 ± 1.4 m, implying that the causative body is 2.0 ± 0.1 m away from the sensor, i.e. at a depth of ~0.8 ± 0.1 m. The first section is comparable with the depth extent of the burnt material observed during small excavations at the site (Figure 3b). The second linear section (ii) suggests a body 0.2 m from the sensor, but this probably relates to the 'wobble' in the position of the sensor during continuous data acquisition. The third section (iii) has a very low gradient, and most-likely corresponds to ambient magnetic noise.

The higher amplitude magnetic anomalies (> ±100 nT/m) observed in the Grad601 grid could be responses from larger fragments of ferrous wreckage, but a further survey would be required to evaluate the size and/or depth of these potential targets.

This interpretation is greatly strengthened by the XRF spectrometry. Co-located with the magnetic anomalies are local geochemical anomalies, particularly evident for elements (copper and zinc) associated with brass. Besides iron and aluminium, brass is the most significant metallic component of the fully-armed Mosquito aircraft. The geochemical evidence is particularly compelling since, in the absence of other information, the air-crash is the most plausible means of introducing these elements into the ground at this location; by contrast, the burnt layer alone could be more simply explained by (for example) disposal at some point in the recent history of the site. The full suite of geophysical and geochemical observations is therefore consistent with an air crash at the site identified within Nuthampstead Airfield.

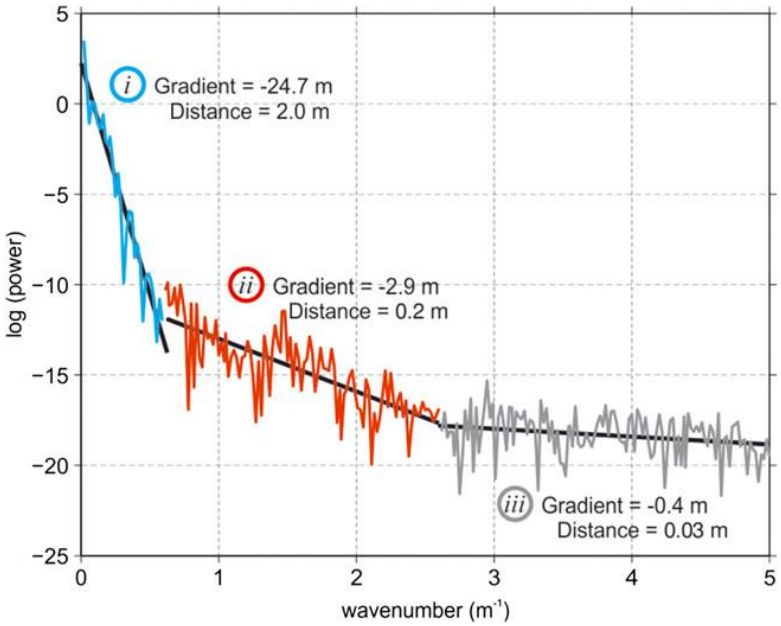

FIGURE 10 Power spectrum of magnetic field strength, recorded by the upper sensor of the G-858 gradiometer. Linear section i (fit to blue data) expresses a gradient of -24.7 m, corresponding to a depth of 0.8 m for the associated causative body. Linear sections ii (fit to red data) and iii (fit to grey data) are assumed, respectively, to correspond to elevation variations of the sensor and ambient noise [Colour figure can be viewed at wileyonlinelibrary.com]

4.2 | Efficacy of in situ XRF surveying

To use in situ XRF surveying as an archaeological exploration tool, some mechanism must exist to transport 'exotic' (i.e. absent in the background) geochemical elements from their buried source to the ground surface. No metallic fragments were observed in the laboratory-powdered soil samples, suggesting that elements at the site are transported in groundwater rather being present in shards of metallic debris.

At Nuthampstead, ploughing appears to be an effective transport mechanism, and the time since ploughing appears to be a key control on the clarity of the XRF anomalies. The survey in November 2014 was conducted soon after a period of ploughing, potentially supplying the ground surface with a 'fresh charge' of metal-rich groundwater. Anomalies and their correlation coefficients were both reduced in the August 2015 dataset (e.g. Figure 8) compared to November 2014. Ordinarily, it might be expected that the drier ground conditions in summer would yield higher geochemical concentrations (e.g. Schneider et al., 2016) but, at the time of this acquisition, the ground had been undisturbed for several months. Metal ions could therefore have been flushed from the site by (for example) rainfall, or transported back into the subsurface. However, some ions must also remain adsorbed onto soil grains, otherwise, XRF analysis of dry soil (including in the laboratory analyses) would have detected no geochemical anomaly at all. Given that the sample size of the XRF instrument is ~1 cm2, it is unlikely that analyses are conducted at precisely the same location between different time periods; however, the changes in the XRF responses are not a shift in the position of the geochemical anomalies, but in the scatter and

the correlation of geochemical concentrations. Separate to instrumental effects (e.g. calibration and sensitivity), the measured concentrations are therefore a function of:
a. the abundance of a given element in the source material,
b. the groundwater solubility and adsorption potential of that given element,
c. the efficiency of any source-to-surface transport mechanism.
Calibration issues are often unavoidable in archaeological XRF surveying (e.g. Scott et al., 2016). A non-specialist should therefore consider XRF spectrometry as a qualitative tool for 'anomaly spotting', rather than interpreting the absolute values of the recorded concentrations. Bespoke calibrations are recommended if absolute concentrations are required (for example) for comparative archaeometric purposes (Scott et al., 2016) or where forensic analysis may lead to litigation (Bergslien, 2013; Ruffell & Wiltshire, 2004; Sbarato & Sánchez, 2001). Validation with laboratory analysis is also advocated since XRF scattering effects are minimized in powdered samples; furthermore, such samples represent a homogenized volume of material, therefore the measurement is less susceptible to 'skin' anomalies.
With respect to the efficiency of acquisition, in situ XRF spectrometry compares favourably with established geophysical methods. Not only is the cost of equipment similar to many geophysical systems, the rate of data return (40 samples/hour, here distributed across a 100 m transect) is comparable to (for example) surveying with electrical resistivity tomography. While XRF spectrometry would probably be impractical as an initial reconnaissance tool, it can contribute valuable insight to the understanding of a target once that target has been identified.

5 | CONCLUSIONS

In situ XRF spectrometry provided a valuable geochemical complement to a suite of geophysical field acquisitions. Localized increases in the concentration of diagnostic metallic elements improved the detectability of the crash site of a World War II aircraft, adding confidence to the interpretation of a suite of geophysical data. Specifically, increases in the local abundance of copper and zinc were identifiable as originating with brass ammunition cartridges among the aircraft wreckage. The applicability of in situ XRF at a given site requires not only that anomalous elements are present in detectable abundance, but that some source-to-surface transport mechanism (e.g. ploughing) is active. While in situ XRF responses should be validated under laboratory conditions, the portable XRF spectrometer offers a useful complement to a programme of field geophysical survey.

ACKNOWLEDGEMENTS

This work is dedicated to the memory of Plt. Off. Raymond Payne and Fg. Off. John 'Dunch' McMillan of 487 Squadron Royal New Zealand Air Force. The late Farmer Martin Barker allowed access to the Nuthampstead site, and Jayne Rollo assisted with field acquisition during 2015. Andrew Kyprianou and Stephanie Trayhurn assisted with logistics. The manuscript benefitted from the constructive comments of two anonymous reviewers.

REFERENCES

Aidona, E. V., Sarris, A., Kondopopulou, D., & Sanakis, I. (2001). Application of magnetic and spectrometry methods in the detection of human activity in soils: A case study at the archaeological site of Kitros (northern Greece). Archaeological Prospection, 8, 187–198. https://doi.org/10.1002/arp.168.

Bergslien, E. T. (2013). X-ray diffraction and field portable X-ray fluorescence analysis and screening of soils: project design. In D. Pirrie, A. Ruffell, & L. A. Dawson (Eds.), Geological Society Special Publication No. 394Environmental and Criminal Geoforensics. London: The Geological Society.

Berlin, J. (2011). Analysis of boron with energy-dispersive X-ray spectrometry: Advances in light element analysis with SDD technology. Imaging & Micrometry, 13, 19–21.

BGS. 2014. Borehole record TL43NW39 (BGS ID 19536802), completed 12 June 2014 at Morrice green Farm, Nuthampstead. http://scans.bgs.ac.uk/sobi_scans/boreholes/19536802/images/19536797.html (accessed 30 March 2016).

Bonizzoni, L., Bruni, S., Guglielmi, V., Milazzo, M., & Neri, O. (2011). Field and laboratory multi-technique analysis of pigments and organic painting media from an Egyptian coffin (26th dynasty). Archaeometry, 53(6), 1212–1230.

Campana, S. (2009). Archaeological site detection and mapping: Some thoughts on differing scales of detail and archaeological 'non-visibility'. In S. Campana, & S. Piro (Eds.), Seeing the Unseen: Geophysics and Landscape Archaeology. FL: Taylor and Francis chapter 2.

Carey, C. J., Wickstead, H. J., Juleff, G., Anderson, J. C., & Barber, M. J. (2014). Geochemical survey and metalworking: Analysis of chemical residues derived from experimental non-ferrous metallurgical processes in a reconstructed roundhouse. Journal of Archaeological Science, 49, 383–397.

Cook, S. R., Banerjea, R. Y., Marshall, L.-J., Fulford, M., Clarke, A., & van Zwieten, C. (2010). Concentrations of copper, zinc and lead as indicators of hearth usage at the Roman town of Calleva Atrebatum (Silchester, Hampshire, UK). Journal of Archaeological Science, 37(4), 871–879.

Cultrone, G., Molina, E., Grifa, C., & Sebastián, E. (2011). Iberian ceramic production from Basti (Baza, Spain): First geochemical, mineralogical and textural characterization. Archaeometry, 53(2), 340–363.

Del Solar Valarde, N., Kinis, S., Chapoulie, R., Joannes-Boyau, R., & Castillo, L. J. (2016). Characterization of pre-Columbian artefacts in situ through handheld portable X-ray fluorescence spectrometry: The case of ceramics from the Mochica site of San José de Moro (Peru). Heritage Science, 4(37). https://doi.org/10.1186/s40494-016-0109-y.

Dirix, K., Muchez, P., Degryse, P., Mušič, B., & Poblome, J. (2013). Integrating multi-element geochemical and magnetic survey at ancient Sagalassos (southwest Turkey): Anthropogenic versus natural anomalies. Arcaheological Prospection, 20, 233–247.

Dungworth, D. B. (1997). Roman copper alloys: Analysis of artefacts from northern Britain. Journal of Archaeological Science, 24, 901–910.

Falcone, R., Renier, W., & Vertià, M. (2008). Wavelength-dispersive X-ray fluorescence analysis of ancient glasses. Archaeometry, 44(4), 531–542.

Fernandes, R., van Os, B. J. H., & Huisman, H. D. J. (2013). The use of handheld XRF for investigating the composition and corrosion of Roman

copper-alloyed artefacts. Heritage Science, 1(30). https://doi.org/10.1186/2050-7445-1-30.
Forster, N., Grave, P., Vickery, N., & Kealhofer, L. (2011). Non-destructive analysis using pXRF: Methodology and application to archaeological ceramics. X-Ray Spectrometry, 40, 389–398.
Frahm, E. (2013). Validity of 'off-the-shelf' handheld portable XRF for sourcing near eastern obsidian chip debris. Journal of Archaeological Science, 40, 1080–1092.
Hall, G. E. M., Bonham-Carter, G. F., & Buchar, A. (2014). Evaluation of portable X-ray fluorescence (pXRF) in exploration and mining: Phase 1, control reference materials. Geochemistry – Exploration Environment Analysis, 14, 99–123.
Hanesch, M., Stanjek, H., & Petersen, N. (2006). Thermomagnetic measurements of soil iron minerals: The role of organic carbon. Geophysical Journal International, 165, 53–61 https://doi.org/10.111/j.1365-246X.2006.02933.x.
Hedges, R. E. M., & Millard, A. R. (1995). Bones and groundwater: Towards the modelling of diagenetic processes. Journal of Archaeological Science, 22, 155–164.
Herz, N., & Garrison, E. G. (1998). Geological Methods for Archaeology; Part II – Dating Techniques. Oxford: Oxford University Press.
Jones, G. (2001). Geophysical investigation at the Falling Creek ironworks, an early industrial site in Virginia. Archaeological Prospection 8: 247–256. https://doi.org/10.1002/arp.173
Krause, M. O. (1979). Atomic radiative and radiationless yields for K and L shells. Journal of Physical and Chemical Reference Data, 8(2), 307–327.
Lu, A. X., Wang, J. H., Pan, L. G., Han, P., & Han, Y. (2010). Determination of Cr, cu, Zn, Pb and as in soil by field portable X-ray fluorescence spectrometry. Spectroscopy and Spectral Analysis, 30(10), 2848–2852 https://doi.org/10.3964/j.issn.1000-0593(1010)10-2848-05.
McKenzie, A. B., & Pulford, I. D. (2002). Investigation of contaminant metal dispersal from a disused mine site at Tyndrum, Scotland, using concentration gradients and stable Pb isotope ratios. Applied Geochemistry, 17 (8), 1093–1103.
McNeill, J. D. (1983). Technical Note TN-11: Use of EM31 Inphase Information. Mississauga, Ontario: Geonics Limited.
Millard, A. R. (1999). Geochemistry and the early alum industry. Geoarcaheoology: Exploration, Environments, resources, Geological Society Special Publication No. 165. The Geological Society: London; 139–146.
Osgood, R. (2014). Exercise Tally Ho! – Archaeological Project Report for the Recovery of Spitfire P9503 at Lidbury, near Upavon, Wiltshire, under the Protection of Military Remains Act (1986). Historic England: Manchester.
Potts, P. J., Webb, P. C., & Williams, T. O. (1997). Investigation of a correction procedure for surface irregularity effects based on scatter peak intensities in the field analysis of geological and archaeological rock samples by portable X-ray fluorescence spectrometry. Journal of Analytical Atomic Spectrometry, 12, 769–776.
Pye, K., & Croft, D. (2007). Forensic analysis of soil and sediment traces by scanning electron micrometry and energy-dispersive X-ray analysis: An experimental investigation. Forensic Science International, 165 (1), 52–63.
Quye-Sawyer, J., Vandeginste, V., & Johnston, K. J. (2015). Application of handheld energy-dispersive X-ray fluorescence spectrometry to carbonate

studies: Opportunities and challenges. Journal of Analytical
Atomic Spectrometry, 30, 1490–1499.
Ruffell, A., & Wiltshire, P. (2004). Conjunctive use of quantitative and qualitative
X-ray diffraction analysis of soils and rocks for forensic analysis.
Forensic Science International, 145(1), 13–23.
Sbarato, V. M.,&Sánchez, H. J. (2001). Analysis of arsenic pollution in groundwater
aquifers by X-ray fluorescence. Applied Radiation and Isotopes, 54
(5), 737–740 https://doi.org/10.1016/S0969-8043(00)00349-3.
Schneider, A. R., Cancès, B., Breton, C., Ponthieu, M., Morvan, X., Conreux,
A., & Marin, B. (2016). Comparison of field portale XRF and aqua regia/
ICPAES soil analysis and evaluation of soil moisture influence on FPXRF
results. Journal of Soils and Sediments, 16, 438–448 https://doi.org/
10.1007/s11368-015-1252-x.
Schwertmann, U., & Taylor, R. M. (1989). Iron oxides. In Minerals in Soil
Environments (second ed.SSSA Book Series, 1) (pp. 379–438). Madison,
WI: Soil Science Society of America.
Scott, R. B., Eekelers, K., & Degryse, P. (2016). Quantitative chemical analysis
of archaeological slag material using handheld X-ray fluorescence
spectrometry. Applied Spectroscopy, 70(1), 94–109 https://doi.org/
10.1177/0003702815616741.
Sepúlveda, M., Gutierrez, S., Carcamo, J., Oyaneder, A., Valenzuela, D.,
Montt, I., & Santoro, C. M. (2015). In situ X-ray fluorescence analysis
of rock art paintings along the coast and valleys of the Atacama
Desert, northern Chile. Journal of the Chilean Chemical Society, 60(1),
2822–2826.
Shugar, A. (2013). Portable X-ray fluorescence and archaeology: Limitations
of the instrument and suggested methods to achieve desired results. In
R. A. Armitage, & J. H. Burton (Eds.), Symposium on Archaeological Chemistry:
American Chemical Society, Division of the History of Chemistry.
Washington, DC: American Chemical Society.
Speakman, R. J., Little, N. C., Creel, D., Miller, M. R., & Inanez, J. G. (2011).
Sourcing ceramics with portable XRF spectrometers? A comparison
with INAA using Mimbres pottery from the American southwest.
Journal of Archaeological Science, 38, 3483–3496.
Spector, A., & Grant, F. S. (1970). Statistical models for interpreting
aeromagnetic data. Geophysics, 35, 293–302.
Środoń, J., Drits, V., McCarty, D. K., Hsieh, J. C. C., & Eberi, D. D. (2001).
Quantitative X-ray diffraction analysis of clay-bearing rocks from
random preparations. Clays and Clay Minerals, 49, 514–528.
Tjallingil, R., Röhl, U., Kölling, M., & Bickert, T. (2007). Influence of the water
content on X-ray fluorescence core-scanning measurements in soft
marine sediments. Geochemistry, Geophysics, Geosystems, 8(2),
Q02004. https://doi.org/10.1029/2006GC001393.
VittoriAntasari, L., Cremonini, S., Desantis, P.,Calastri, C.,&Vianello, G. (2013).
Chemical characterisation of anthro-technosols from bronze to middle age
in bologna (Italy). Journal of Archaeological Science, 40(1), 3660–3671.
Weltje, G. J., & Tjallingil, R. (2008). Calibration of XRF core scanners for
quantitative geochemical logging of sediment cores. Earth and Planetary
Science Letters, 274, 423–438.
White, H., & Dungworth, D. (2007). Warmley Brassworks, Siston, Bristol:
Analysis of Some Eighteenth-century Brassworking Debris, Historic
England Report, Heritage Protection Department, Report 54/2007.
Historic England: Manchester.
Wilson, C. A., Davidson, D. A., & Cresser, M. S. (2008). Multi-element soil

analysis: An assessment of its potential as an aid to archaeological interpretation. Journal of Archaeological Science, 35(2), 412–414.
SUPPORTING INFORMATION
Additional Supporting Information may be found online in the supporting information tab for this article.